Dielectric Properties of Silver Borogermante Superionic Glassy System

F. M. Hafez

Physics Department, Faculty of Science, Al -Azhar University, Girls Branch, Cairo, Egypt
mg_hafez52@hotmail.com

Abstract: The superionic system xAgI – (100-x) [Ag_2O-0.5 GeO_2–B_2O_3] series 1 and 50AgI–20Ag_2O–y GeO_2–(20–y) B_2O_3 series 2 where x=10, 20, 30, 40, 50 and 60% and y= 0, 5, 10, 20, 30 % have been prepared by rapid melt quenching technique. The samples were investigated by x-ray diffraction to check its amorphous nature. No diffraction peaks were observed in XRD patterns at room temperature indicating their amorphous structure. However for x=60% few microdomains are observed, so it consider as a composite. The Ac measurements were carried out over the frequency rang (42Hz –5MHz). The addition AgI enhances ionic conduction where it generates easy path for conducting ions. These glasses exhibit high ionic conductivity (10^{-3} S/cm at x=50%). i.e. the samples behave as super ionic conducting glass. The present systems exhibit time dependent conductivity, confirming ionic conduction which is the dominant conduction mechanism. The conductivity increases with increasing AgI content. However, the addition of GeO_2 leads to (almost independent) conductivity. Different dielectric relaxation processes, electrode polarization, translational polarization and rotational polarization are considered in the present system. The studies reveal the drastic decrease of electronic component and increase of the ionic by the addition of AgI. This presumably is caused by formation of Ag^+ conductive "tissue" facilitated by a considerably disrupted glass network.
[Hafez FM. **Dielectric Properties of Silver Borogermante Superionic Glassy System**. *Nat Sci* 2013;11(3):13-25]. (ISSN: 1545-0740). http://www.sciencepub.net/nature. 3

Keywords: Superionic glass, dielectric relaxation, permittivity, ionic conductivity

1. Introduction

The study of superionic solids is an important field of material science and technology. The conduction of solid is based on motion of electron. In contrast ionic solids have received very little attention in the past, in spite of fact that these solids are the best to be understood by solid state physicist and chemists. The main reason for this was the non availability of solids with high ionic conductivity at room temperature.

Solids with high ionic conductivity are termed as "superionic solids" or solid electrolytes. The so called glassy electrolytes or superionic glasses have been produced and studies due to their high ionic conductivity at room temperature and for their relative ease of preparation in several shapes and compositions [(1)]. In field of ionic conductors the glass has several advantages in comparison with the crystal in the same composition.

The glassy electrolytes are a class of materials in which the cationic or anionic constituents are not confined to specific lattice site, but are essentially free to move throughout the structure. Thus, these classes have attracted much attention because of their use for application in solid state electrochemical devices such as rechargeable batteries or micro battery operation, which needed for electric automobiles and heart pacemakers, fuel cell electrochromic devices, electrochemical sensor, smart windows and displays [(2)].

Ionic conductors in non – crystalline solids are called in several ways; glassy or vitreous electrolytes, fast ion conducting glasses (FIC), superionic conducting glasses (SIC) superionic glasses (SI) and so on.

AgI based borate and germante glasses have attracted much attention because of high glass transition temperature [(3)].

2. Experimental work

2.1. A homogenous mixture of chemicals in appropriate mol wt compositions

x AgI–(100–x) [Ag_2O–0.5 GeO_2–B_2O_3] series 1, 50Ag1–20Ag_2O–y GeO_2–(20–y) B_2O_3 series 2 where x= 10, 20, 30, 40, 50, 60% and y= 0, 5, 10, 20, 30%. The samples were prepared from pure chemical compounds, $AgNO_3$ (Aser 99.99), B_2O_3 (Aldrich 99.99) GeO_2 (Aldrich 99.99), silver nitrate was used as source material for yielding silver oxide. AgI was prepared by reacting KI and $AgNO_3$ in dionized water [(4)]. The mixture was melted in porcelain crucible at 600-750^{o}C for 25-30 min depending on composition. The melts were shaken several times during heating to ensure a high degree of homogeneity, and then the melts were quenched between two polished copper blocks kept at room temperature to yield the homogeneous glasses.

The samples were examined to test the amorphous nature using BUKER axs X-ray analytical diffraction system, type D8 ADVANCE supplied with furnace attachment. The diffraction system

based with Cu tube anode of wave length $K\alpha_1$= 1.5460 Å and $K\alpha_2$= 1.54439 Å. The start angle (2θ) was 10° and the end angle was 60°.

The dielectric constant ε`, dielectric loss ε``, tangent loss tan δ and the a.c. conductivity as a function of frequency were estimates R, C using a programmable automatic RCL meter (Hioki RCL Z3531 High Tester, RS-232C, version 1.31).

The experimental measurements were carried out over the frequency range (42Hz-5.0MHz). When the parallel equivalent circuit is used, the real part of dielectric is the dielectric constant, ε' was calculated as:

$$\varepsilon' = \frac{t}{A}\ \frac{C}{\varepsilon_o} \qquad (1)$$

where t is the thickness of the sample in m units, A is the cross section area in m^2 units, C is parallel capacitance of the sample in Farad units and ε_o is the permittivity of free space (ε_o=8.85x10^{-12} F/m). Also the imaginary part, ε'' represents the dielectric loss was calculated as:

$$\varepsilon'' = \varepsilon'.\tan\delta \qquad (2)$$

The complex impedance Z* can be defined as:

$$Z^* = \frac{t}{A}\ \rho^* \qquad (3)$$

where ρ^* is the complex resistivity, and the real and imaginary part of impedance can be calculated as:

$$Z' = Z''.\tan\delta \qquad (4)$$

$$Z'' = 1/(\omega C(1+\tan\delta)^2)) \qquad (5)$$

The complex electronic modulus M* can be defined as:

$$M^* = 1/\varepsilon^* \qquad (6)$$

The real and imaginary part of dielectric electronic modulus, M', M'' respectively was calculated as:

$$M' = 1/(\varepsilon'(1+(\tan\delta)^2)) \qquad (7)$$

$$M'' = M'.\tan\delta \qquad (8)$$

3. Results and Discussion

3.1. X-ray diffraction

Representative X-ray diffraction (XRD) patterns at room temperature are illustrated in Fig. (1). No sharp peaks are observed, reflecting the amorphous nature of the prepared samples except at x=60%. The XRD pattern of x = 60% (sample) shows intense peaks due to β-AgI are observed as well as peaks which may be due to α-AgI at room temperature[5]. Hence the x=60% sample can be considered as composite.

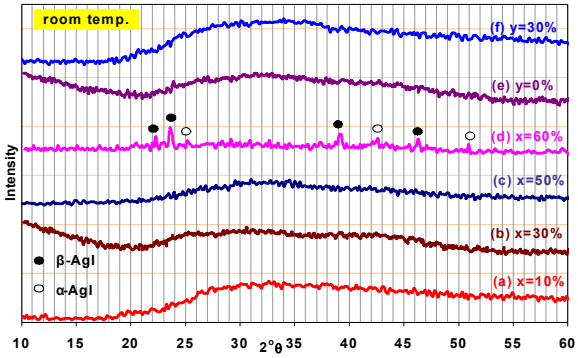

Figure 1. X-ray diffraction pattern for some samples at room temperature.

3.2. Conductivity measurements

3.2.1. Frequency dependence of the total conductivity

The dependence of log σ_{tot} on log ω over frequency range 42Hz-5MHz in temperature range 24-120°C were measured, Fig. (2) represents the obtained data of x=50%. The spectra follow the known pattern of fast ionic conductors (FIC) [6]. Generally the frequency dependent conductivity plots at various temperatures show two main distinct regions: an almost frequency independent plateau region at low frequencies followed by a region of continuous increasing conductivity at higher frequencies, the conductivity relaxation region. The intersection of the two regions gives ω_p, where ω_p is the hopping rate of mobile ions. In the present system Ag^+ is mobile ions. ω_p shows a shift by raising the temperature. The conductivity also increases by increasing temperature. This may be due to the increase of ions mobility.

In disordered systems the charge transport takes place due to hopping conduction. Moreover the motion of a charge is accompanied by an electrical relaxation: ionic and electronic charges surrounded by negative and positive charge. A hope of a charge carrier to a new site can only lead to a successful charge transport if the polarization cloud follows.

Otherwise the charge carriers will jump back with a high probability. This mutual movement of the charge carriers and the surrounding polarization cloud requires an electrical relaxation time t_σ. If the frequency of the external electrical field is higher than $1/t_\sigma$ it affects the charge transport average out.

For frequency lower than $1/t_\sigma$ the relaxation of the polarization cloud is in phase with the outer filed [7].

As the frequency is further raised the permanent dipoles, will be completely unable to follow the external field and orientation polarization ceases and then frequency independent [8]. The appearance of this region is postponed by increasing temperature and/or AgI content.

At lower frequency region, the increase of the conductivity indicates electrode polarization (space charge) [6,7]. This behavior becomes more pronounced at higher temperatures and by increase AgI content Figs. (2) and (3). This may be attributed to the increased number of defects and / or AgI formed clusters.

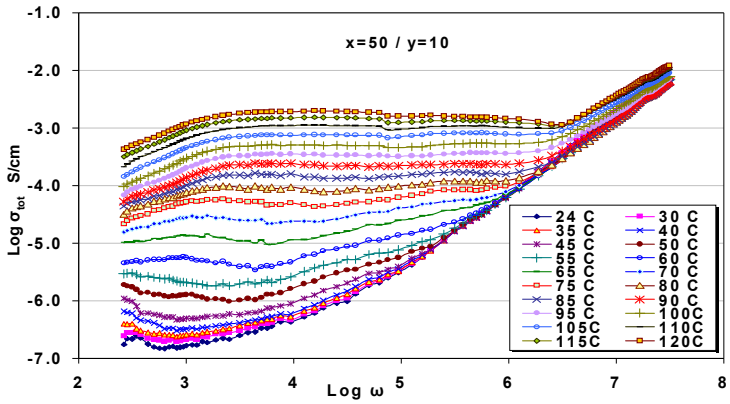

Figure 2. Typical total conductivity frequency dependence at different temperatures for x=50 % / y=10% sample.

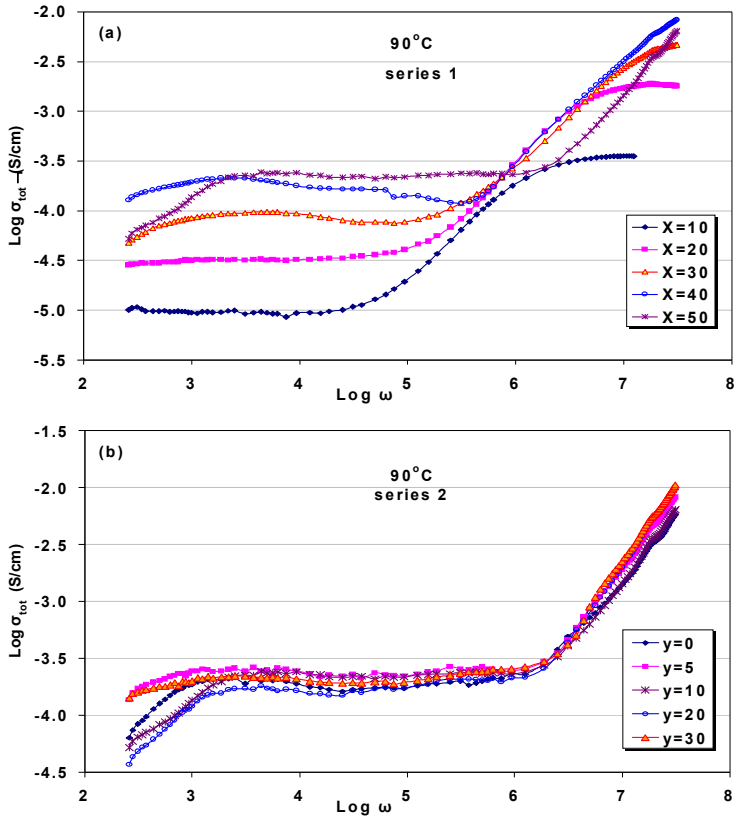

Figure 3. Total conductivity frequency dependence at different compositions for (a) series 1 and (b) series 2 at 90°C.

The hopping frequency is assumed to be a thermally activated parameter as, in case of practical solid electrolytes, then it should follow the relation [9]:

$$\omega_p = \omega_0 \exp(\frac{-E_m}{KT}) \quad (9)$$

where ω_p is the effective attempt frequency where $\omega_p = \omega_o$ at T= ∞ K and E_m is the free energy of migration of the mobile ions. The value of E_m is obtained by the least square fitting of equation (9) as shown in Fig. (4). It is clear that, for x $\geq$ 40% Ln ω_p against 1/T curves show two distinct regions, the transition takes place (at ~60°C) may be due to the formation of α-AgI nanocrystals which increase with increasing AgI as it is clear from XRD results [10,11,12].

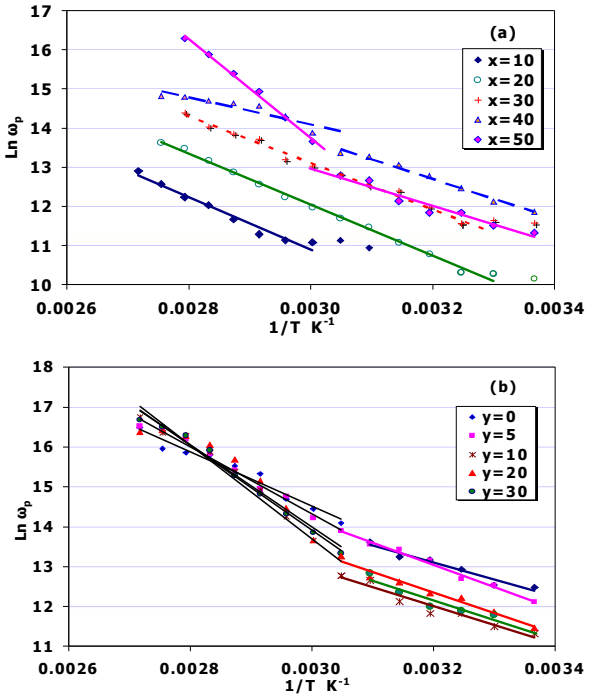

Figure 4. Ln ω_p as a function of 1/T for both systems.

Fig. (5.a) represents the E_m values as a function of composition; it is clear that E_m decrease with increasing AgI content. This is expected since the addition of AgI causes two effects, one is the expansion structure as shown in molar volume, the second is that AgI considered as ideal electrolyte because the rigid sublattice of I^- ions, the carrier concentration is high since all of Ag^+ ions are potentially mobile, and the migration of silver ions along pathways established by iodide ions [2,6]. On the other hand in series2 E_m increases with increasing GeO_2.

On the other hand, the calculated relaxation time , τ , at room temperature shows tendency to decrease with increasing AgI content as shown in figure (5.b). This is in consistence with fact that, the addition of AgI enhances polarization response and hence the conductivity. While as, in the series2 τ tend to increase with increasing GeO_2.

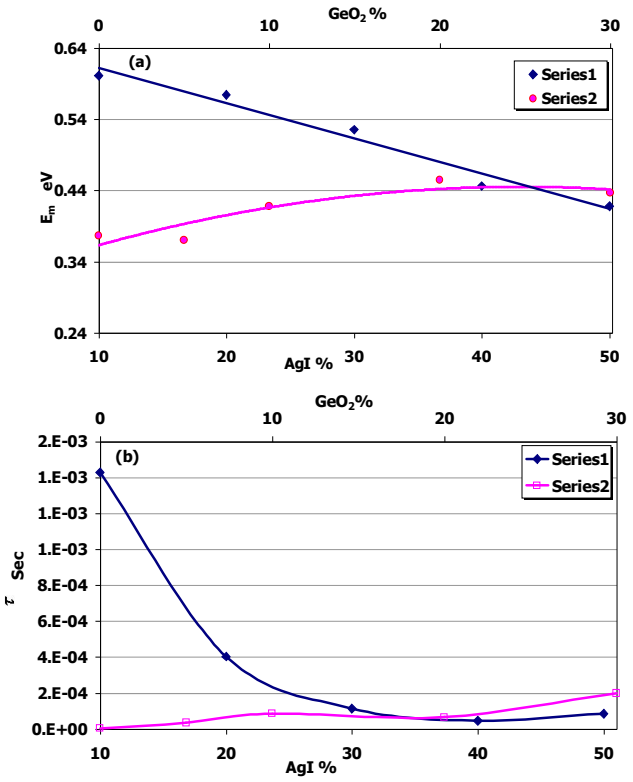

Figure 5. (a) Composition dependence of the free energy of migration (E_m). (b) Composition dependence of relaxation time, τ for two series.

3.2.2. Conduction mechanisms

The dependence of conductivity on the frequency has been analyzed using the power law exponent [9,13]

$$\sigma_{tot}(\omega) = \sigma_{dc} + A\ \omega^S \quad (10)$$

where $\sigma_{tot}(\omega)$ is the total conductivity at a particular frequency, σ_{dc} the dc conductivity at zero frequency, A and s are weakly temperature dependent parameters. In order to account for the mechanism of a.c. conduction, various theoretical models have been appeared in the literature [14,15]. As it is seen from Fig (6), there are two regions of

temperature dependence of s suggesting two different mechanism of conduction.

The value of the exponent's' is higher than unity, such behavior has been reported in some ionic systems, where the addition of AgI leads to an increase of ionic component of electrical conduction [16,17]. For x=10% the values of s increases with temperature up to ~80°C and then s temperature independent. The small polaron tunneling as well as the atomic quantum mechanical tunneling model proposed by Elliot were used to interpret the conductivity behavior, respectively.

In the other samples, the atomic quantum mechanical tunneling (from room temperature to ~70°C) as well as the correlated barrier hopping (above 70°C) where s increase with increasing temperature is used to interpret the conductivity behavior [14].

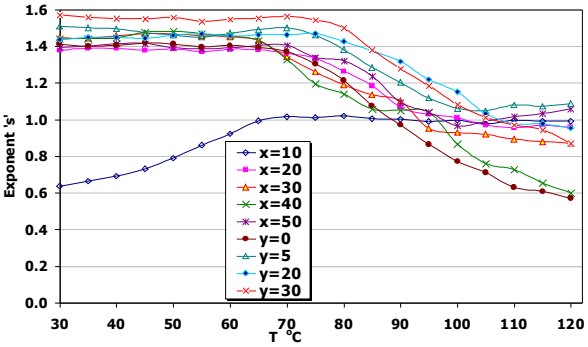

Figure 6. Temperature dependence of the frequency exponent's.

3.2.3. Time dependence of the total conductivity

The time dependence of the total conductivity for all investigated samples at 100 Hz is shown in Fig. (7). It is observed that, all samples follow one common pattern, where σ_{room} decays almost exponential with the time, which is a feature of ionic conductors. This is most likely due to the migration of conducting species towards the negative electrodes. At the same time, the initial values shows increase with increasing AgI content, having values of order ~10^{-3} S/cm for x=50%. This makes prepared systems good candidates as solid state or superionic electrolytes. One may assume that these materials exhibit ionic conduction with negligibly small electronic conductivity contribution [18]. Figure (8.a) show an increase of the conductivity with increasing AgI, this is most likely due to the increase of conducting ions Ag^+ and/ or the role of iodide in enhancing conductivity by raising mobility.

On the other hand the time dependence of the conductivity tends to decrease with increasing GeO_2 in series2 due to an increasing of the compactness, as illustrated in figure (8.b).

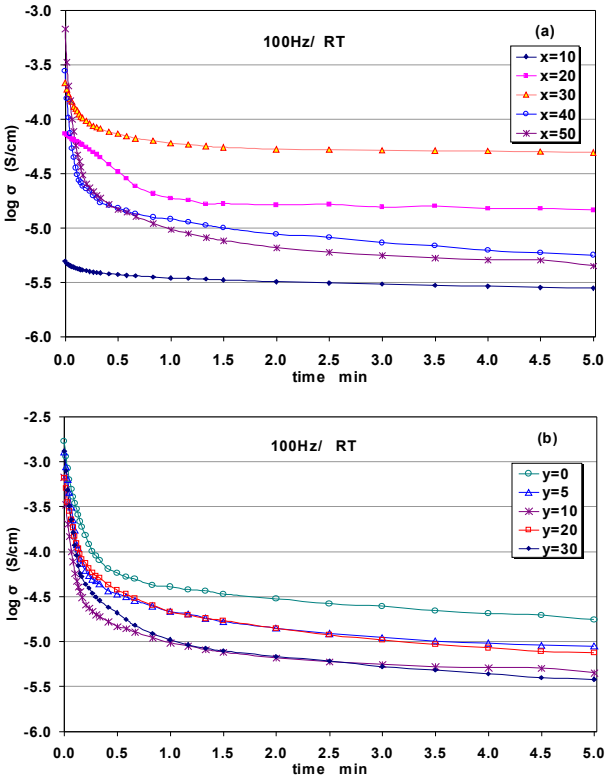

Figure 7. The σ_{tot} time dependence at 100Hz and at room temperature.

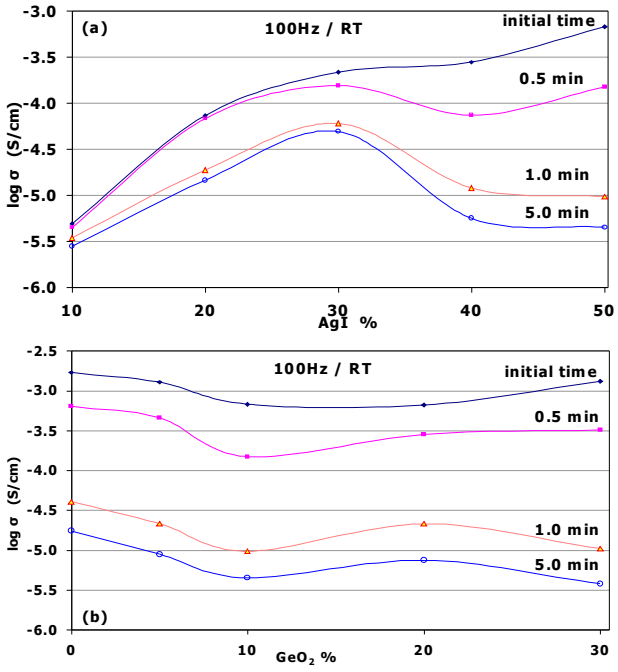

Figure 8. The σ_{tot} at 100Hz and at room temperature as a function of, (a) AgI, (b) GeO_2 content.

The observed decay is more pronounced for high AgI content, which means that silver ions migrate along easy pathways generated and established by I ions, this is attributed to the Ag^+ carrier which are potentially mobile by the I ions [2,19]. Hence, the dynamical models of the conducting Ag^+ ion center on two possible modes of transport; that the ions pass between vacant sites in a homogenous network, or that they are transported via small connected clusters of AgI [20,21].

The increasing of AgI content enhances mobile ions movement hence, rate of decay increases. On the other hand, the increasing of GeO_2 content rate of decay decreases due to increasing of the compactness of the network.

3.2.4. Composition dependence of the total conductivity

The composition dependence of total conductivity is represented in Fig. (9) at 100 Hz and different temperatures. By increasing AgI the total conductivity tends to increases for x=10-50% instead of a decrease for x=40-50% at room temperature as shown in Fig. (8). Such results can be explained as follow: at lower temperatures, a group of Ag^+ ions (especially from Ag_2O) are attaching themselves to the non-bridging oxygen's with strong partial covalency; this group of ions is termed the 'immobile' carriers. Whilst Ag^+ ions surrounded by halide ions represent the 'mobile' carriers and the third are Ag^+ ions interacting with BO_4 and/or GeO_6 groups. With increasing temperature; some of the immobile convert into mobile ions, especial with increasing AgI content, and vice versa [12,22]. It appears that the increase in the conductivity is based on the reduction of the network rigidity and the decrease of the T_g. [6].

One could therefore explain the conductivity or ion migration of these ordinary glasses simply by using a well-defined thermal activated ion hopping process, ignoring the unsuccessful hopping or trapping because the probability of these events is very small [6]. Hence, by heating the glassy samples, the total conductivity increases, where some of the immobile ions convert into mobile ions. At the same time by the introduction of AgI, conductivity has increased exponentially especially at higher frequency [23,24].

The composition dependence of the total conductivity in series2 at different frequencies and temperatures is shown in figure (9.b), by the introduction of GeO_2 content there is almost conductivity independent, this may be due to mobile ion saturation effect or decrease of easy pathways.

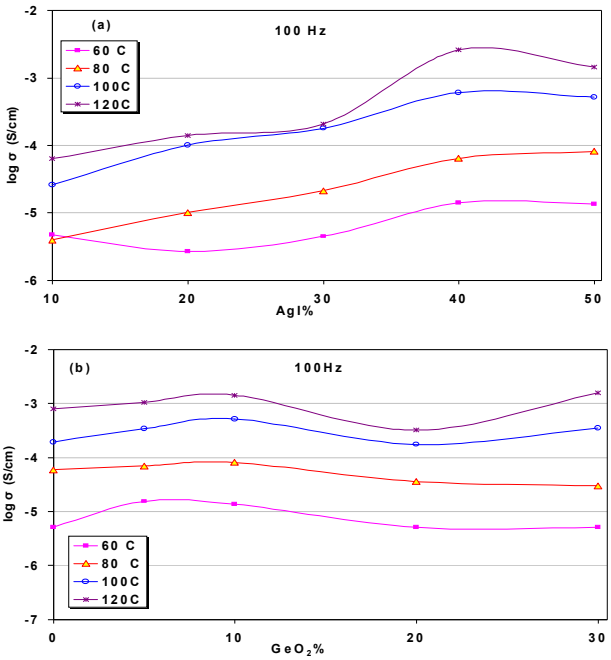

Figure 9. σ_{total} as a function of (a) AgI, (b) GeO_2 at 100 Hz.

3.3. Dielectric measurements

3.3.1 Dielectric loss tangent (tan δ)

Figs. (10) and (11) show the frequency dependence of the dielectric loss tangent (tan δ) at various temperatures for the investigated samples. The relatively large values of tan δ confirm the important contribution of DC conductivity to the dielectric permittivity [25]. All samples follow one common pattern, where at low frequencies a peak is observed at given frequency F_{max}. Such peak position shifts to higher frequency by increasing temperature, indicating a thermally activated process. This behavior indicates dielectric dispersion characterized by relaxation frequency F_{max} [25]. At higher frequencies, second peak appears at x=10 and 20% which shifted toward higher frequency by increasing temperature. This peak follows Deby relaxation [8]. At high AgI content, splitting in tan δ occurs by increasing temperature may be due to the formation of α -AgI nanocrystals or microdomains which is consultant with XRD results. The activation energy was estimated by plotting log F_{max} versus 1/T as shown in Fig. (12) according to:

$$F_{max} = F_o \exp(\Delta E / kT) \qquad (11)$$

where k is the Boltezman constant, ΔE is the activation energy.

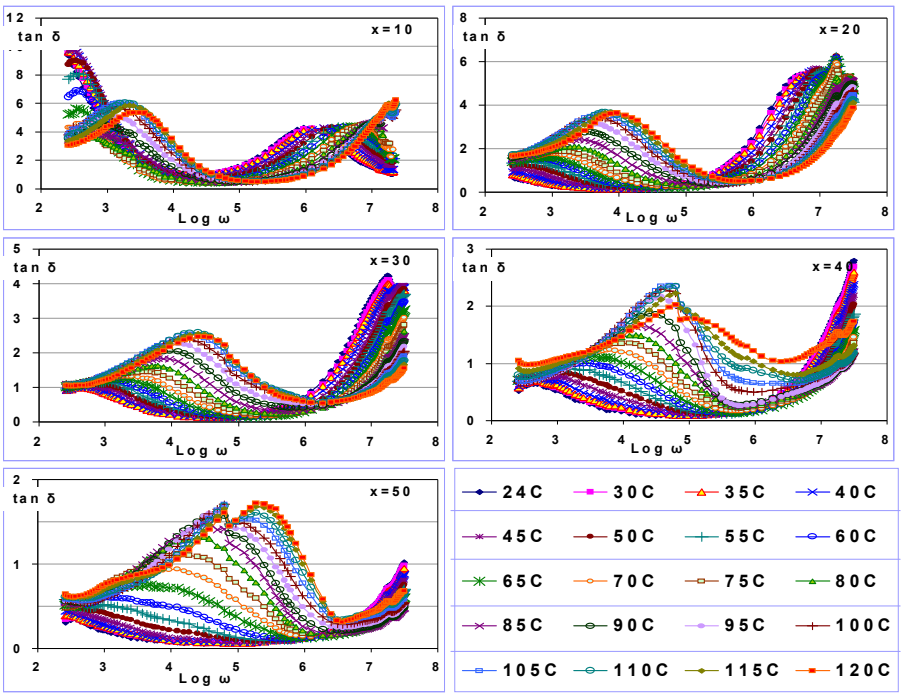

Figure 10. tan δ frequency dependence for series 1.

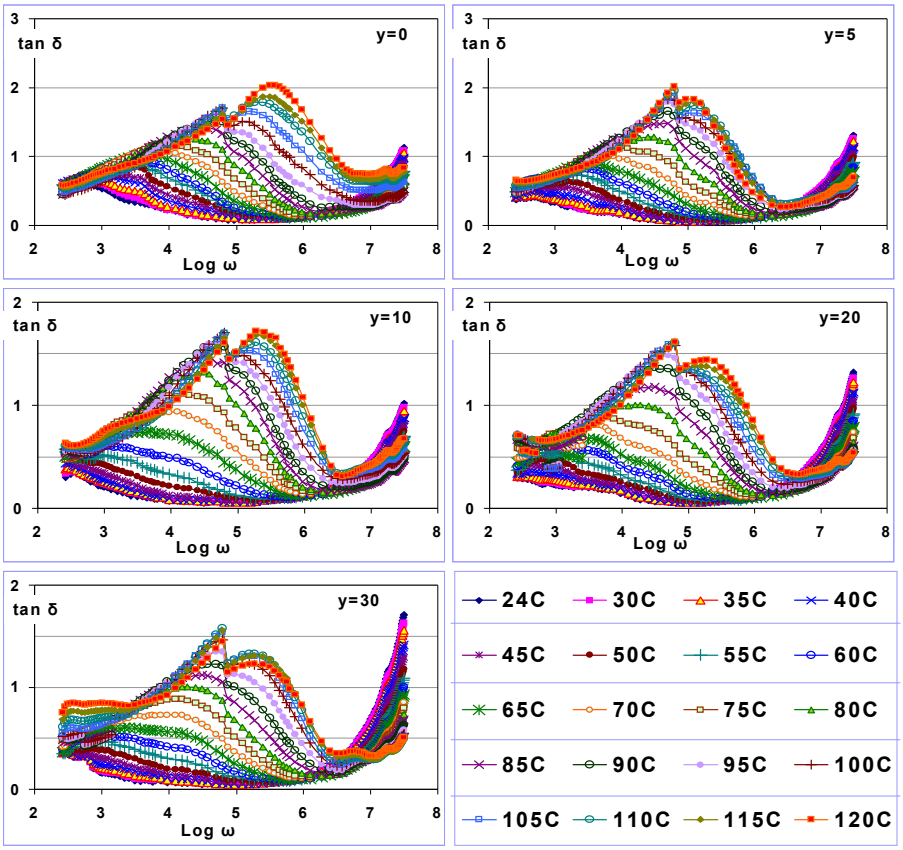

Figure 11. tan δ frequency dependence for series 2.

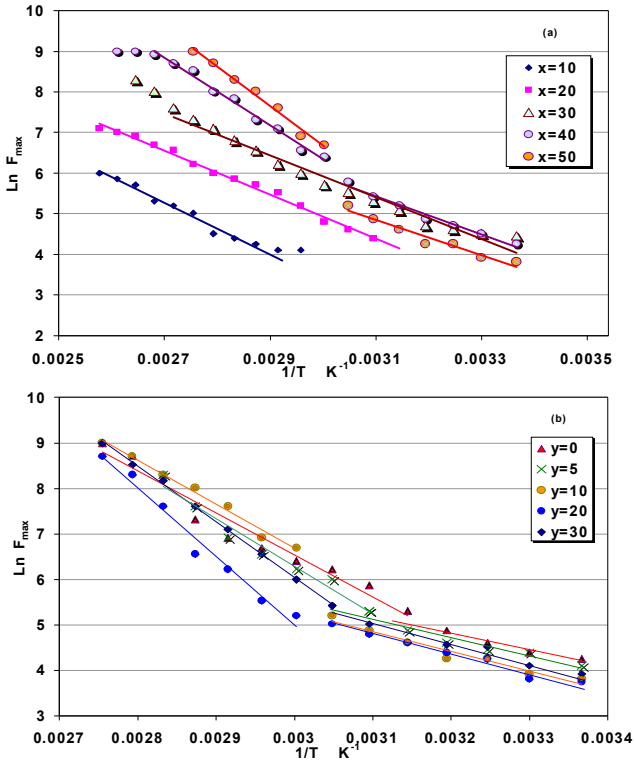

Figure 12. Ln F_{max} as a function of 1/T for two series.

On the other hand log(F_{max}) temperature dependence show two distinct regions, the transition between these regions are located at ~ 60-70°C as shown in Fig. (12), this may be attributed to the formation of α -AgI nanocrystals or microdomains by increasing AgI. The existence of such α -AgI domains, especially at higher AgI concentration are recently confirmed by Raman, NMR and neutron diffraction scattering results [10,26,11].

Fig. (13) shows the activation energy as a function of the composition. It is clear that, the activation energy decreases with increasing AgI content which agree with above arguments concerning conductivity. Also it show increase with increasing GeO_2 content this is related to the fact that addition of GeO_2 reduces the number of easy pathways.

3.3.2. Dielectric permittivity

Fig. (14) represents the relation between the ε'' in logarithmic scale and ε' as a function of frequency for x=30% as representative spectra. Generally, the dielectric permittivity show strong frequency dependence.. Three relaxation processes are involved in the dielectric permittivity for all the investigated samples[7]. The first process at low frequency, ε', ε'' decrease by increasing frequency. The separation of charges at interfaces which gives rise to an additional polarization at the external electrodes contacting the sample on a macroscopic scale. Also this process can take place at inner dielectric boundary layers (Maxwell/Wagner/Sillars-polarization) on a mesoscopic scale. The latter is the dominant mechanism at low frequency, and termed as the electrode or interfacial polarization[7]. The second process is locate at moderate frequency, ε' is almost frequency independent, while as the ε'' exhibit sharp decrease with increasing frequency which transformed into a peak tan δ. This is known as the conduction contribution or the translation diffusion of ions. The third process at relatively high frequencies, the decreases of ε' with increasing frequency represents anomalous dielectric dispersion relaxation. Whilst the variation of ε'' with frequency is termed the relaxation absorption characteristic of the dielectric, ε'' represents a dielectric loss and hence an absorption of energy [7,8,27], this decrease transformed into peak in tan δ in this frequency region. The latter obeys Deby-type dielectric dispersion [8].

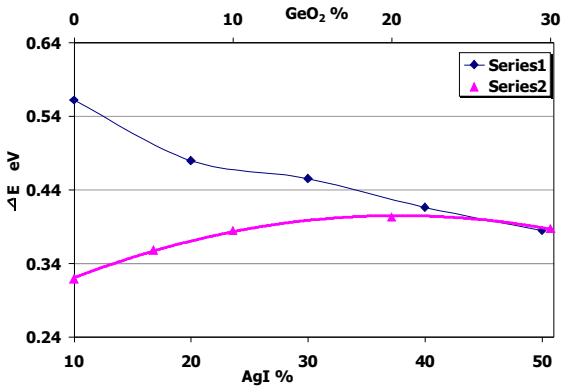

Figure 13. Activation energy composition dependence.

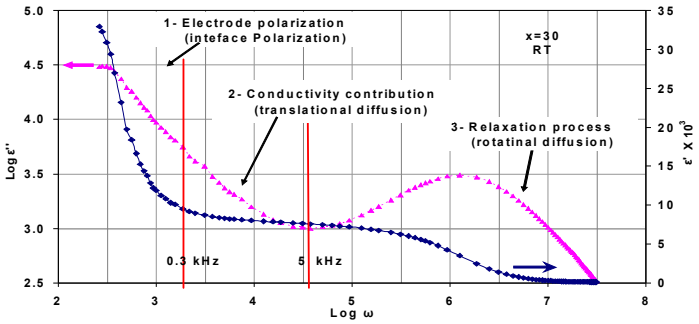

Figure 14. Frequency dependence of the ε' (solid line), and ε'' (dashed line), of dielectric permittivity at room temperature for x=30 %.

The relaxation phenomenon includes rotational diffusion of molecular dipoles in the microscopic scale at high frequency. It is observed that the peak in ε'' is shifted towards higher frequency by increasing temperature. In the other word it represents a thermally activated process.

Fig. (15) shows typical real and imaginary parts of dielectric permittivity frequency dependence respectively, at different temperatures for x=30%. All samples show common behavior as shown in Figs. (16) and (17) for both systems where a peak in ε'' is shifted towards higher frequency by increasing AgI content.

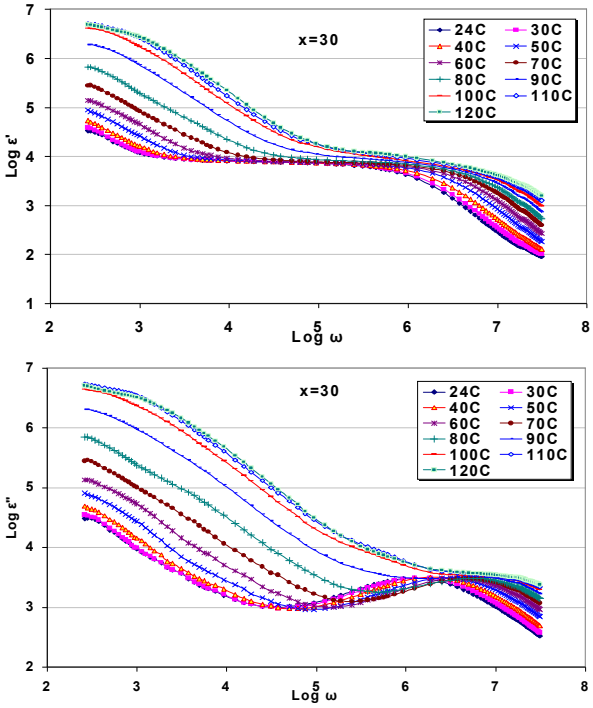

Figure 15. Typical frequency dependence of the ε', and ε'' of the dielectric permittivity at different temperatures for x=30%.

Figs. (18) and (19) show the composition dependence of the real and imaginary dielectric permittivity at different temperatures for the two series respectively. By increasing temperatures some of immobile ions convert in to mobile ones to enhance the conduction phenomenon. However by increasing GeO_2 the two parts of dielectric are almost composition independent. At low temperature, by increasing AgI, ε'' show decrease and then increase at high AgI content, i.e. exhibit the conductivity behavior. Due to the conductivity is proportional directly to ε'' to confirm the conduction contribution process.

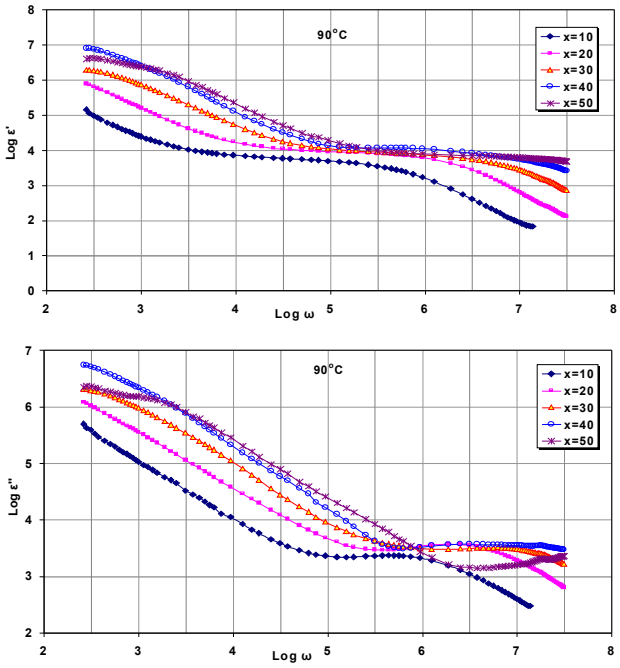

Figure 16. Frequency dependence of the Log ε', and Log ε'' of the dielectric permittivity at 90°C for series 1.

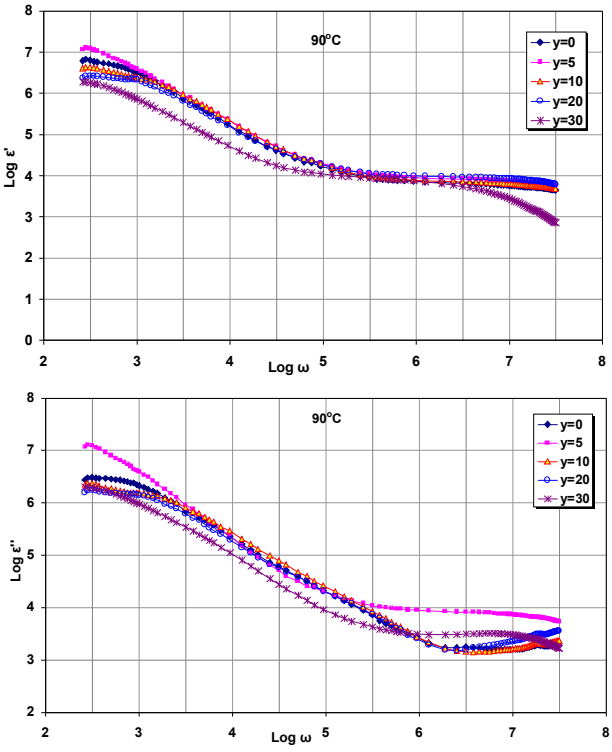

Figure 17. Frequency dependence of the Log ε', and Log ε'' of the dielectric permittivity at 90°C for series 2.

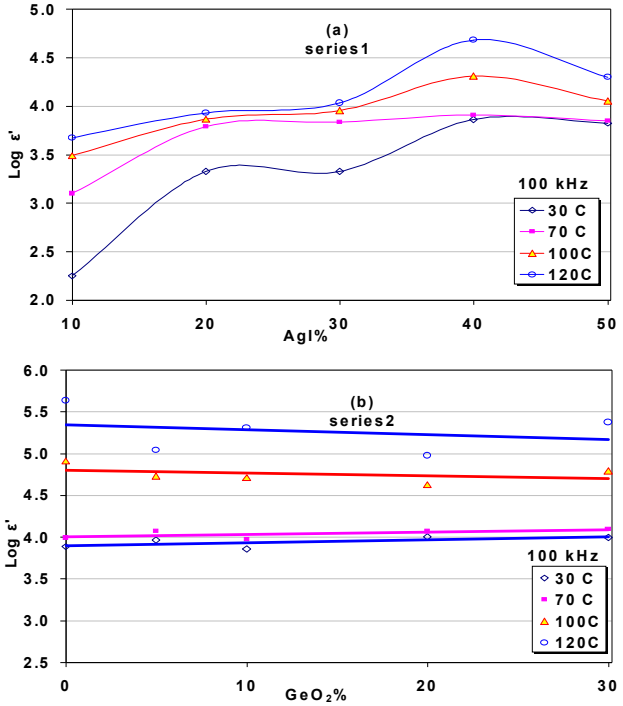

Figure 18. Real dielectric, Log $\mathcal{E}$', composition dependence at different temperatures & 100 kHz (a) series 1 and (b) series 2.

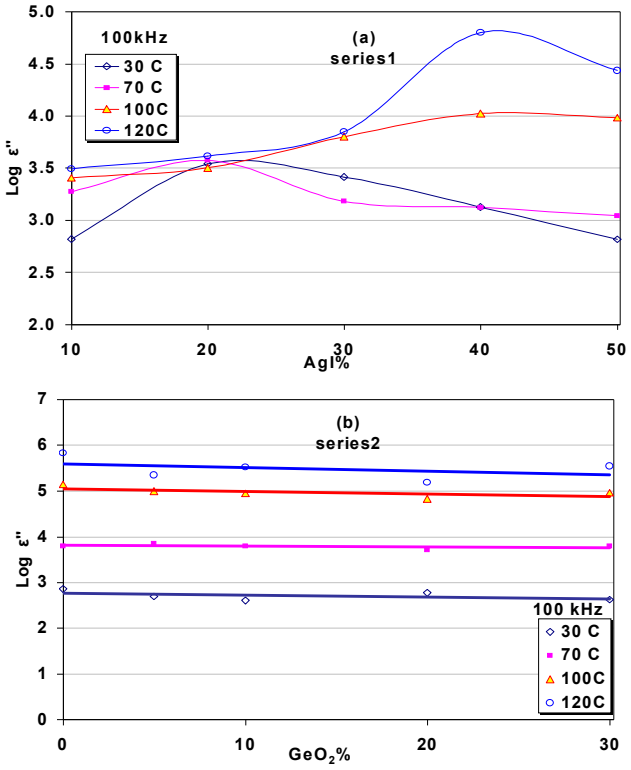

Figure 19. Imaginary dielectric ,Log $\mathcal{E}$ '', composition dependence at different temperatures & 100 kHz (a) series1and (b) series 2.

3.4. Complex impedance

The impedance spectrum of a polycrystalline material is expected to show two semicircular arcs; one attributed to the bulk and the second to the grain boundary effects. A third semicircle corresponding to the sample/electrode interface may also exist [25,28,29]. The above mechanisms were observed in the AgI based glasses corresponding to the existence of AgI nanocrystals in the glass.

Fig. (20) shows typical Z'-Z'' diagram for x=10% at room temperature as representative spectra. It describes two semicircle arcs the first represents bulk glass region and the second represents electrode region [25,28,29]. The obtained result is related to series connection of two parallel circuits R_bC_b and $R_{elect.}C_{elect.}$ where; $C_b << C_{elect.}$ and $R_{elect} >> R_b$ where C_b , R_b are capacitance and resistance according to bulk glass region and $C_{elect.}$, R_{elect} are capacitance and resistance according to electrode region respectively. The two semicircle on the complex impedance diagram are well separated and the resistance corresponding to the bulk (dc) conductivity can be determined by the intersection of the impedance arc with the real impedance axis, $R_{b,}$ as shown in Fig. (20). This spectrum is similar to those observed for conductors with two types of charge carries, mixed electronic and ionic conduction, with pronounced diffusion effects in the electrode region [17].

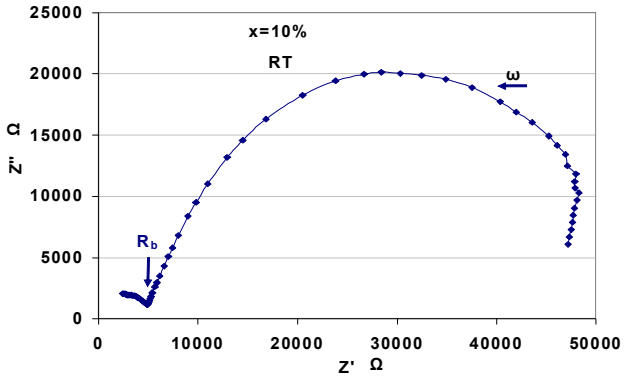

Figure 20. Imaginary part of impedance Z'' versus real part of impedance Z' at room temperature for x=10%.

A representative complex impedance plan plot used to determine the bulk conductivity. Fig. (21) show this plot for x=10% at different temperatures. It is clear that, due to the high conduction nature of this systems, the relaxation frequency of bulk property are expected to be very high, so the bulk resistance effects would be observed at very high frequency only [28,30]. It is found that the semicircle is slightly depressed, and it likely arises from the dielectric relaxation of ions or other kinds of

relaxation such as contact polarization. As the temperature is increased, the impedance decreases, and it is seen that the bulk response arcs partially disappear with increasing temperature. This makes the determination of bulk conductivity difficult to be observed at high frequencies because, in some cases, the arc is completely absent. The dc conductivity in this case was determined by extrapolation the polarization 'spike' in the complex plan to the intersection with the real impedance axis [6]. However the same effect were observed by increasing AgI content as shown in Fig. (22). For x>10%, the spectrum is typical for almost purely ionic conductors [17]. On the other hand there are arc located at low frequency, this arcs will be discussed later in the dielectric modulus section.

The obtained bulk conductivity of ionic glass is found to be thermally activated; for the ionic materials, the temperature dependence of conductivity obeys the well know relation [28,31,32]:

$$\sigma_b T = \sigma_o \exp(-\Delta E / kT) \qquad (12)$$

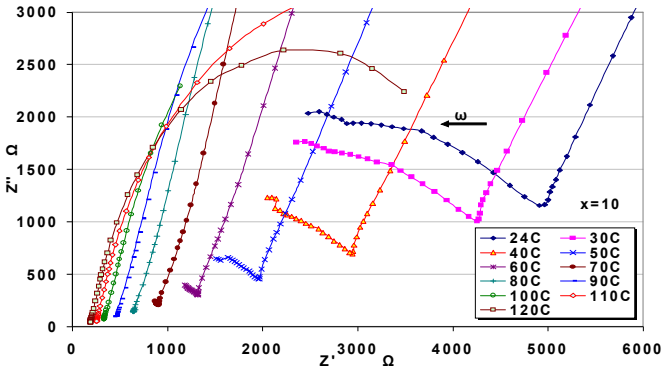

Figure 21. Imaginary part of impedance Z'' versus real part of impedance Z' at different temperature for x=10 %.

where Δ E is the activation energy and k is the Boltezman constant. The obtained bulk conductivity as a function of 1/T in K^{-1} is presented in Fig. (23) for two series, the activation energy decrease with increasing AgI. While it is almost independent with increasing GeO_2 content or tends to increase as in Fig. (24). Fig. (25) shows the bulk conductivity composition dependence at different temperatures for both systems. By increasing AgI the bulk conductivity increases linearly while, tend to decrease in series 2.

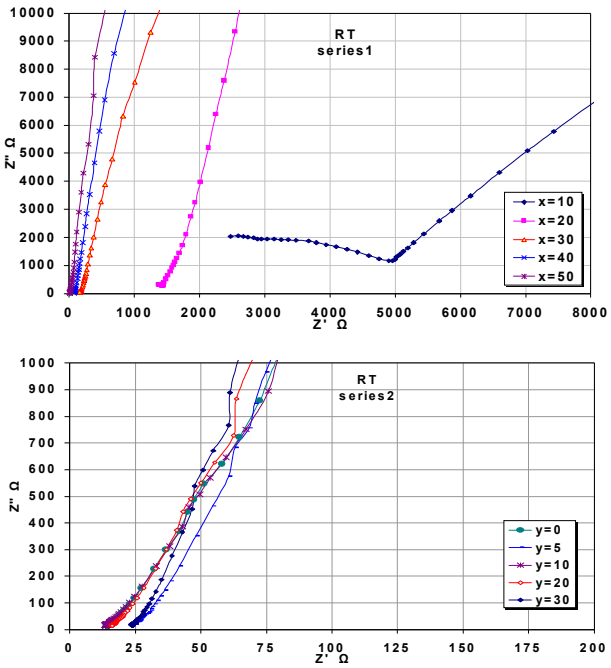

Figure 22. Imaginary part of impedance Z'' versus real part of impedance Z' at room temperature, (a) series 1 and (b) series 2.

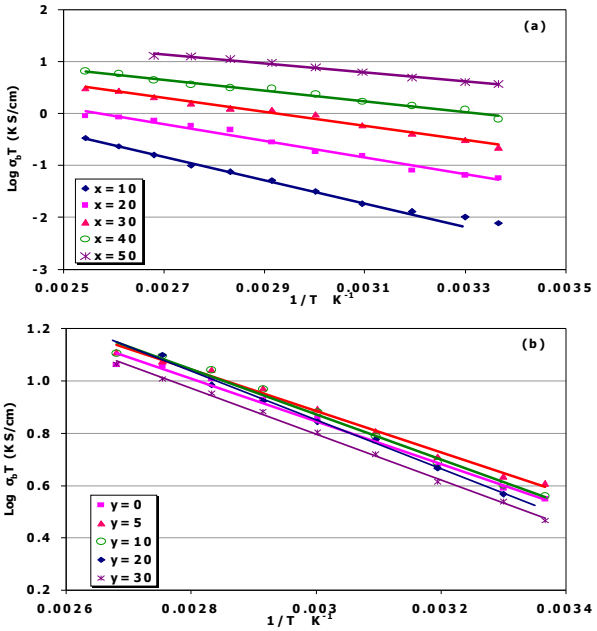

Figure 23. The Log σ_bT as a function of reciprocal temperature.

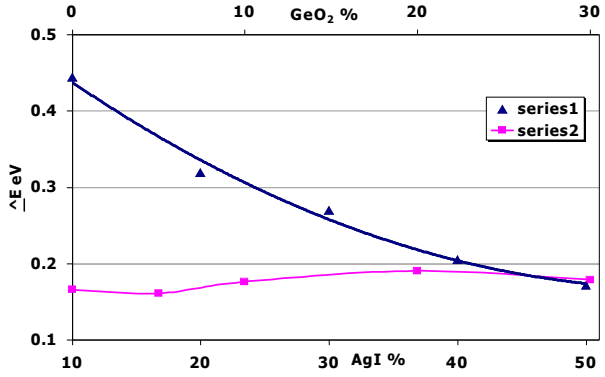

Figure 24. The activation energy composition dependence for all samples.

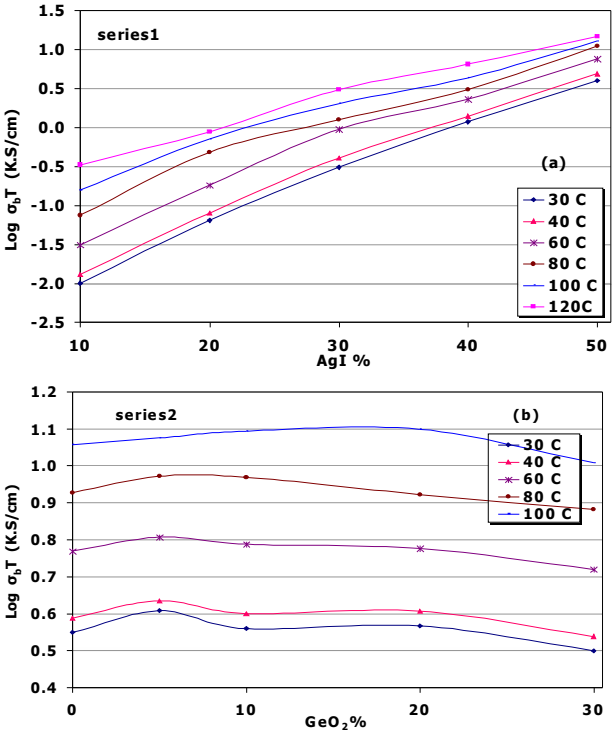

Figure 25. Log $\sigma_b T$ composition dependence for (a) series 1 and (b) series 2.

3.5. Dielectric modulus

Dielectric modulus is parameter which used as modified presentation of the dielectric parameters. It illustrates the polarization and allows study of dielectric relaxation in the relaxation of absence of a well defined dielectric loss peak (in tangent loss) [16]. Fig. (26) shows typical frequency dependence of the real dielectric modulus (M') and imaginary (M") parts at different temperatures for x=30 %. The peak position of the imaginary dielectric modulus was shifted to higher frequency with increasing temperature. The sharp increase of M' and decrease in ε'' with increasing frequency is transformed into a peak in M", this refers to the conduction contribution (mobile charge carries) [7].

The insert figure shows the M"-M' diagram for x=30% at room temperature with two semicircles are observed. The high frequency semicircle corresponds to the bulk conductivity. While the low frequency semicircle represents the highly capacitive but weakly conducing regions (sample/electrode interface) [32].

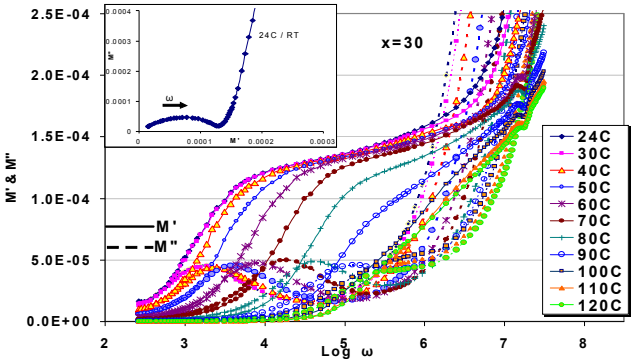

Figure 26. Typical dielectric modulus frequency dependence for x=30 % sample.

4. Conclusion

Superionic systems xAgI-(100-x)[Ag_2O-0.5GeO_2-B_2O_3] and 50AgI-20Ag_2O-yGeO_2-(30-y)B_2O_3 where x=10, 20, 30, 40, 50, 60 % and y=0, 5, 10, 20, 30% have been prepared by melt quenching technique. No diffraction peaks were observed in X-ray pattern of the investigated samples at room temperature indicating their amorphous nature except at x=60% which consider as composite. Peaks due to growth of AgI microdomains are observed in X-ray pattern by increasing temperature and heat treatment. The addition of AgI enhances ionic conduction where it generates easy paths for conducting ions. Such, these glasses show high ionic conductivity which reach to ~ 10^{-3} S/cm at x=50%. So, the samples can be used as superionic glasses. The present systems exhibit time dependent of conductivity, which confirm that the ionic conduction is the dominant mechanism. The conductivity increases with increasing AgI content while as the addition of GeO_2 exhibit opposite trend. Different dielectric relaxation processes, electrode polarization, translational polarization and rotational polarization are found in the both present systems. The impedance studied reveals the drastic decrease of electronic component and increase of the ionic one, on the addition of AgI. This presumably is caused by formation of Ag^+ -

conductive "tissue" facilitated by a considerably disrupted glass network.

Corresponding Author:
F. M. Hafez
Physics Department, Faculty of Science
Al -Azhar University, Girls Branch, Cairo, Egypt
E-mail: mg_hafez52@hotmail.com

References

1. C.S. Sunandana, S. Kumar, Bull. Mater. Sci., V. 27, No. 1 (2004) 1-17.
2. T. Minami, J. of Non-Cryst. Solids, 95 & 96 (1987) 107-118.
3. J.F. Jurado, J.A. Trujillo, B.E. Mellander, R.A. Vargas, Solid State Ionics, 176 (2005) 985-990.
4. J.J. Hudgens, S.W. Martin, Physical Review B, V. 53, No. 9 (1 Mar. 1996) 5348-5355.
5. M. Tatsumisago. T. Saito, T. Minami, Phys. Chem. Glasses, 42(3) (2001) 215-219
6. Q. Mei, Jason Saienga, Jeremy Schrooten , Steve W. Martin J. of Non-Cryst. Solids,168 (2003) 75-85.
7. F. Kremer, A. Schonhals, "Broadband Dielectric Spectroscopy", Springer, Berlin, (2004).
8. A.A. Zaky, R. Hawley, Dielectric Solids, (1970).
9. A. Karki, S. Feller, Hun p. Lim, J. Starr, C. Sanchez, M. Shibata, J. of Non-Cryst. Solids, 92 (1987) 11-19.
10. G. Dalba, A. Fontana, P. Fornasini, G. Mariotto, M.R. Masullo, F. Rocca, Solid State Ionics, 9&10 (1983) 597-602.
11. C. Rousselot, J.P. Malugani, R. Mercier, M. Tachez, P. Chieux, A.J. Pappin, M.D. Ingram, Solid State Ionics, 78 (1995) 211-221.
12. R.C. Agrawal, R. Kumar, J. Phys. D: Appl. Phys., 27 (1994) 2431-2437.
13. K.P. Padmasree, D.K. Kanchan, H.R. Panchal, A.M. Awasthi, S. Bharadwaj, Solid State Communications, 136 (2005)102-107.
14. S.R. Elliot, Adv. Physic. 36 (1987) 135-218.
15. S.R. Elliott, Philosophcial magazine, V. 36, No. 6 (1977) 1291-1304.
16. S. Hazra, A. Ghosh, Physical Review B, V. 55, No. 10 (1 March. 1997) 6278-6284.
17. J.E, Garbarczyk, P. Machowski, M. Wasiucionek, L. Tykarski, R. Bacewicz, A. Aleksiejuk, Solid State Ionics, 136-137 (2000) 1077-1083.
18. R.C. Agrawal, R. Kumar, R.K. Gupta, Materials Science and Engineering B, 57 (1998) 46-51.
19. T. Minami, T. Shimizu, M. Tanaka, Solid State Ionics, 9&10 (1983) 577-584.
20. C. Guy, N. Umesaki, N. Kamijo, M. Tatsumisago, N. Torata, T. Minami, M. Furusaka, Physica B 213 & 214 (1995) 493-495.
21. J. Swenson, R.L. McGreevy, L. Börjesson, J.D. Wicks, Solid State Ionics, 105 (1998) 55-65.
22. T. Minami, J. of Non-Cryst. Solids, 56 (1983) 15-26.
23. T. Minami, K. Imazawa, M. Tanaka, J. of Non-Cryst. Solids, 42 (1980) 469-476.
24. M. Sekine, Y. Suzuki, H. Ueno, Y. Onodera, T. Nasu, S. Wei, J. of Non-Cryst. Solids, 353, 18-21 (2007) 2069-2073.
25. M. Ahmad, K. Yamada, T. Okuda, Physica B 339 (2003) 94-100.
26. N. Kuwata, J. Kawamura, Y. Nakamura, K. Okuda, M. Tatsumisago, T. Minami, Solid State Ionics, 136-137 (2000) 1061-1066.
27. V. Sudarsan, S.K. Kulshrestha, J. of Non-Cryst. Solids, 225 (1999) 228-232.
28. J.R. Dygas, Solid State Ionics, 176 (2005) 2065-2078.
29. D. Fasguelle, J-C. Carru, C. Renard, J. of Non-Cryst. Solids, 353 (2007) 1120-1125.
30. S. Murugesan, A. Wijayasinghe, B. Bergman, Solid State Ionics, 178,11-12 (2007) 779-783.
31. K. Krasowski, J.E. Garbarczyk, M. Wasiucionek, Phys. Stat. Sol. (a), 183, No. 2 (2001) 381-389.
32. M.M. Ahmad, Solid State Ionics, 177(2006) 21-28.

12/16/2012